JGR Atmospheres

RESEARCH ARTICLE
10.1029/2020JD033045

An Energetic View on the Geographical Dependence of the Fast Aerosol Radiative Effects on Precipitation

Guy Dagan[1], **Philip Stier**[1], **and Duncan Watson-Parris**[1]

[1]Atmospheric, Oceanic and Planetary Physics, Department of Physics, University of Oxford, Oxford, UK

Key Points:

- Energy budget perspective is used to examine the latitudinal dependence of the effect of aerosol-radiation interaction on precipitation
- A transition between a positive response in the tropics and a negative response in the extra-tropics occurs at relatively low latitudes
- Scattering and absorbing aerosol effects on precipitation over land and ocean and under more realistic conditions are examined

Supporting Information:

Supporting Information may be found in the online version of this article.

Correspondence to:

G. Dagan,
guy.dagan@physics.ox.ac.uk

Citation:

Dagan, G., Stier, P., & Watson-Parris, D. (2021). An energetic view on the geographical dependence of the fast aerosol radiative effects on precipitation. *Journal of Geophysical Research: Atmospheres*, *126*, e2020JD033045. https://doi.org/10.1029/2020JD033045

Received 5 MAY 2020
Accepted 8 APR 2021

Abstract By interacting with radiation, aerosols perturb the Earth's energy budget and thus the global precipitation amount. It was previously shown that aerosol-radiation interactions lead to a reduction in the global-mean precipitation amount. We have further demonstrated in aqua-planet simulations that the local response to absorbing aerosols differs between the tropics and the extra-tropics. In this study we incorporate an energy budget perspective to further examine the latitudinal-dependence of the effect of aerosol-radiation interaction on precipitation in idealized global simulations. We demonstrate that the transition between a positive local precipitation response in the tropics and a negative local precipitation response in the extra-tropics occurs at relatively low latitudes (~10°), indicating a transition between the deep-tropics (in which the Coriolis force is low, hence direct thermally driven circulation, and associated divergence/convergence of energy/moisture, can form as a result of the diabatic-heating) and their surroundings. In addition, we gradually increase the level of complexity of the simulations and demonstrate that, in the case of absorbing aerosols, the effect of land is to counteract some of the response both inside and outside the deep-tropics due to the reduction in surface latent-heat flux that opposes the diabatic-heating. The effect of scattering aerosols is also examined and demonstrates a decrease in precipitation over land in both the tropics and extra-tropics and no effect over the ocean. Finally, we examine these results in a more realistic set-up and demonstrate that, although the physical mechanisms still operate, they are not significant enough to be discerned from the model's natural-variability.

1. Introduction

Aerosol-radiation interactions are known to drive a slowdown of the hydrological cycle (Ramanathan et al., 2001) due to a reduction in the amount of solar radiation reaching the surface and consequently a reduction in surface fluxes. In addition, absorbing aerosols (such as black carbon) lead to a reduction in the global-mean precipitation due to energy budget conservation. Namely, the atmospheric diabatic heating due to absorbing aerosol is balanced, in the global mean, by a reduction in latent heating by precipitation (Dagan et al., 2019b; Samset et al., 2016). However, previously it was shown that the local precipitation response to an aerosol perturbation in the tropics is opposite of the global mean response and of the extra-tropical response (Dagan et al., 2019b). That is to say that the same idealized aerosol perturbation was shown to decrease precipitation in the extra-tropics and increase precipitation in the tropics. This contrasting response can be explained by the different ability of the atmosphere to diverge excess dry static-energy in the tropics and extra-tropics (Sobel et al., 2001). In the tropics, an atmospheric diabatic heating (e.g., due to absorbing aerosols) leads to a very efficient distribution of the excess energy for large scales (Gill, 1980; Matsuno, 1966), a large-scale direct thermally driven circulation (Roeckner et al., 2006) and thus to a large local increase in precipitation. In contrast, in the extra-tropics, excess energy from aerosol diabatic heating is constrained due to the effect of the Coriolis force, causing the local precipitation to decrease (to maintain energy balance: Dagan et al., 2019b).

Here, we examine the aerosol effect on precipitation from a regional energy budget perspective (Dagan et al., 2019b, 2020; Hodnebrog et al., 2016; Liu et al., 2018; Muller & O'Gorman, 2011; Myhre et al., 2017, 2018; Richardson et al., 2018; Samset et al., 2016). According to this perspective, any aerosol-driven changes in radiation fluxes must be balanced, on long time scales, by changes in precipitation, sensible heat flux or by divergence of dry static energy.

The long-time (monthly time scales and above, for which the atmospheric storage term is small) average total column atmospheric energy budget can be described as follows:

$$LP + Q_R + O_{\mathrm{SH}} = \mathrm{div}(s) \quad (1)$$

Where LP is the latent heat due to precipitation (assuming the condensation occurs at the same horizontal grid point as the precipitation, a valid assumption for coarse resolution global models), Q_{SH} is the surface sensible heat flux, Q_R is the atmospheric radiative heating, and div(s) is the divergence of dry static energy - which will become negligible on sufficiently large spatial scales (Jakob et al., 2019; Dagan & Stier, 2020). Equation 1 provides information on the time mean precipitation rate and not on the distribution of rainfall intensities, which may change under aerosol forcing as well (e.g., Zhao et al., 2019).

Local changes in precipitation due to an aerosol perturbation could be caused by aerosol microphysical effects (Albrecht, 1989; Andreae et al., 2004; Dagan et al., 2015; Khain, 2009; Levin & Cotton, 2009; Liu et al., 2019; Rosenfeld & Lensky, 1998; among many others), by local changes to the energy budget (radiation fluxes or surface sensible heat flux changes) or by changes to the general circulation of the atmosphere, caused by the inhomogeneous aerosol radiative effect (Chemke & Dagan, 2018). For example, asymmetry in aerosol radiative effect between the two hemispheres were shown to leads to cross-equatorial energy flux and thus to a shift in the intertropical convergence zone (Allen et al., 2015; Rotstayn & Lohmann, 2002; Voigt et al., 2017; Wang, 2015). Aerosols-driven changes to the extra-tropical atmospheric circulation may also lead to changes to the spatial distribution of precipitation (Allen & Sherwood, 2011; Chemke & Dagan, 2018; Ming et al., 2011).

In this study we use General Circulation Model (GCM) simulations in two configurations (with and without land) to study the fast precipitation response (with prescribed sea surface temperatures - SST (Bony et al., 2013; Myhre et al., 2018; Richardson et al., 2018)) to idealized and more realistic aerosol perturbation at different locations. The separation into fast (fixed SST) and slow (SST mediated) precipitation responses is useful as the time scales of rapid changes in the atmosphere is much faster than the time scales of changes in SST (Bony et al., 2013; Myhre et al., 2018; Richardson et al., 2018). The set of simulations presented here enable us to expand the analysis presented in Dagan et al. (2019b) in which the differences between the tropics and extra-tropics were demonstrated using idealized global simulations (using aqua-planet configuration and idealized, large aerosol perturbations). This paper addresses the following questions: (1) What latitude does the local precipitation response to absorbing aerosol perturbations shifts from positive in the tropics to negative in the extra-tropics, and why? (2) What is the effect of land on the above-mentioned response, and (3) What is the effect of the spatial structure and magnitude of aerosol perturbation when going from highly idealized to more realistic simulations? Or in other words, can the physical insights from the idealized simulations explain the response under more realistic conditions?

2. Methodology

2.1. Model

The ICON (icosahedral nonhydrostatic) atmospheric GCM (Crueger et al., 2018; Giorgetta et al., 2018; Zängl et al., 2015) is used in aqua-planet and AMIP (Atmospheric Model Inter-comparison Project (Gates, 1992)) configurations. For both the aqua-planet and AMIP simulations we use a grid with resolution of ∼160 km (R2B04 (Zängl et al., 2015)) and 47 vertical levels.

Aerosol radiative effects are represented through the idealized MACv2-SP plume model (Max Planck Institute Aerosol Climatology version 2, Simple Plume (Kinne et al., 2013; Stevens et al., 2017)). This relatively simple aerosol model prescribes the anthropogenic aerosol optical depth (AOD) and its radiative properties (the single scattering albedo–SSA, and the asymmetry parameter), as functions of time, geographical location and wavelength. The aerosol characteristics in MACv2-SP are based on long term observations (Kinne et al., 2013; Stevens et al., 2017). The vertical distribution of aerosol is also based on climatological data set (Kinne et al., 2013) and is parameterized by a kernel of Euler's β function (see details in Stevens et al., 2017). We note that differences in the vertical plume profile may cause different responses of the climate system and general circulation (Ban-Weiss et al., 2012; Kim et al., 2015; Ming et al., 2010; Persad et al., 2012). Here, we use a vertical structure based on long-time average climatological data set showing a general reduction from the low altitudes (the source) to the mid-troposphere (the aerosols are mostly confined to below 5 km). Due to the exponential decrease of pressure with height, profiles of extinction (not of mixing ratios) are

often bottom heavy. There is no coupling between aerosol and cloud microphysics, i.e., only the aerosol radiative effect is considered. For more details about MACv2-SP the reader is referred to Stevens et al. (2017).

2.2. Aqua-Planet Simulations

Nine simulations are conducted in the aqua-planet configuration–one reference simulation with no aerosol forcing, and eight simulations with different aerosol plume centers between 0° and 70° in continues increments of 10°. As in Dagan et al. (2019b), the reference simulation is run for 10 years (to account for natural variability), while each of the perturbed simulations are run for 4 years and reach a stationary-state. The SST is prescribed to be zonally symmetric and to follow:

$$\mathrm{SST} = \begin{cases} 273 + \frac{27}{2} \cdot \left(2 - \left(\sin\left(3 \cdot \frac{\mathrm{lat}}{2}\right)\right)^2 \cdot \left(1 + \left(\sin\left(3 \cdot \frac{\mathrm{lat}}{2}\right)\right)^2\right)\right) & \text{for } -\frac{\pi}{3} < \mathrm{lat} < \frac{\pi}{3} \\ 273 & \text{otherwise} \end{cases}$$

Where lat is the latitude (Rast, 2018). The surface temperature is presented in Figure S1.

In the aqua-planet simulations, we use an idealized and strong aerosol perturbation with a simple Gaussian spatial distribution around the plume center (Dagan et al., 2019b). The radius (standard deviation) of the tropical plume is set to 10° in both the north-south and east-west directions. As in Dagan et al. (2019b), the AOD magnitude at the center of the tropical plume is equal to 2.4, which is the global sum of all plumes in the default MACv2-SP setup, i.e., a very strong local perturbation (Figures S2–S3, present the spatial and horizontal AOD distribution for the idealized cases). We correct for the different width of a degree longitude and for the differing amounts of incoming solar radiation between the different simulations with the different aerosol plume locations. We do that by increasing the plume zonal dimensions and the AOD magnitude at the center of the plume by a factor of 1/cos (lat), where lat is the latitude of the plume center. Hence, for each simulation the global mean perturbation is similar regardless of the plume location. The SSA in this case is set to 0.8.

2.3. AMIP Simulations

In the AMIP simulations, each simulation is run either for 10 (idealized perturbations) or 30 (more realistic perturbations) years. The surface temperature used in this configuration is presented in Figure S1. For the idealized perturbation simulations, we use similar plume characteristics as in the aqua-planet simulations (radius of 10° and AOD = 2.4, Figures. S2–S3). The plume center is located either at the tropics (0°, for three different longitudes, two over land and one over the ocean) or at the extra-tropics (40°, for three different longitudes, two over land and one over the ocean, Figure 1). For each plume location two different SSA of 0.8 and 1 are used.

For the more realistic perturbations we use the default MACv2-SP setup, either including the entire global distribution of aerosol (Full plume) or specific regional plumes. These plume characteristics are based on long-term observations (Kinne et al., 2013; Stevens et al., 2017). Each simulation was conducted for 30 years. In the Full plume simulation the AOD in each plume changed with time according to the MACv2-SP setup for the years 1979–2009.

3. Results

3.1. The Latitudinal Dependence of the Fast Aerosol Effect on Precipitation

To identify the latitude of the transition between the positive local precipitation response due to an absorbing aerosol perturbation in the tropics and the negative local response in the extra-tropics we use the aqua-planet simulations with a stepwise change in the aerosol plume location. Figure 2 presents the atmospheric radiative heating (Q_R) perturbation generated in these simulations, while Figure 3 presents the relative precipitation response (the absolute precipitation response is presented in Figures S4–S5). As expected, for all latitudes the presence of absorbing aerosols generates a positive Q_R perturbation. The magnitude of

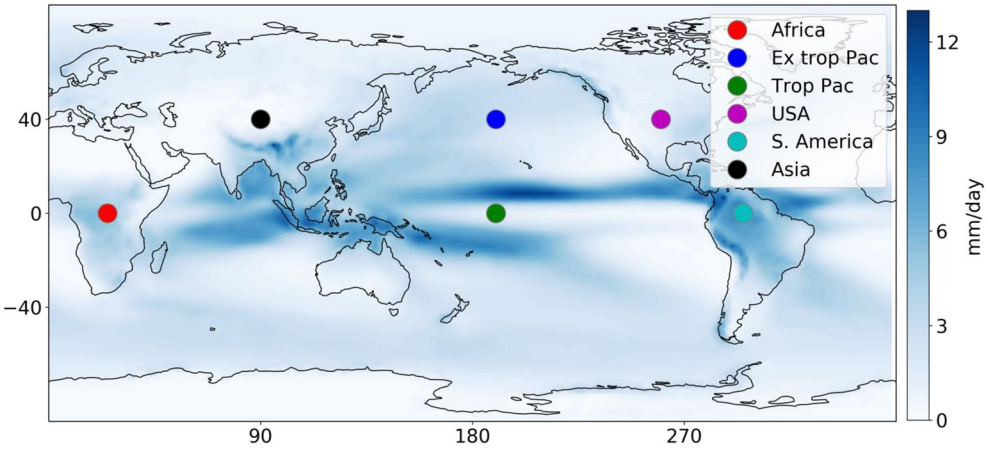

Figure 1. The locations of the aerosol plume centers for the AMIP simulations forced with the MACv2-SP aerosol model. The background represents the time-average surface precipitation over the 30 years simulation in the reference case (no anthropogenic aerosols). AMIP, Atmospheric Model Inter-comparison Project; MACv2-SP, Max Planck Institute Aerosol Climatology version 2 Simple Plume.

the Q_R perturbation slightly decreases with latitude due to the clouds' response to the Q_R perturbation–i.e., deeper clouds formation in the tropics and hence reduction in the outgoing longwave flux and larger Q_R perturbation compared to the extra-tropics (Dagan et al., 2019b). The local precipitation response to this positive Q_R perturbation is positive in the tropics (0° and 10°) and negative in the extra-tropics (30° and above–see also Figure 4 presenting the precipitation response around the center of the aerosol plume as a function of the location of the plume). The simulations in which the aerosol plume center is located at 10° and 20° demonstrates an increase in precipitation at the south part of the plume and a small or even negative response at the north part (Figure 3). At the plume center, the precipitation response is slightly positive for the simulation with the plume center at 10° and negative for the simulation with the plume center at 20° (Figure 4).

Examining the meridional cross-sections of the precipitation response at the longitude of the plume center (Figure 5) demonstrates that the transition between a positive precipitation response at the tropics and a negative response outside the tropics occurs at roughly 10°. This result indicates that the latitude of the transition between the different responses is at fairly low latitudes, and that the positive response occurs only in the deep-tropics where the Coriolis effect is negligible.

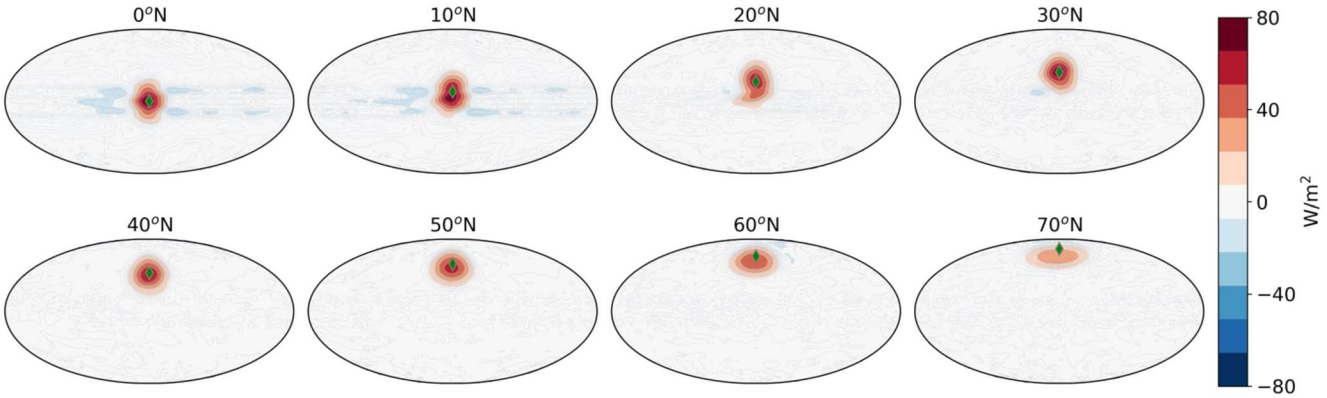

Figure 2. The atmospheric radiative heating (Q_R) perturbation (each simulation minus the reference simulation) in the aqua-planet simulations. For each simulation the aerosol plume center is indicated in the title and is marked by a green diamond.

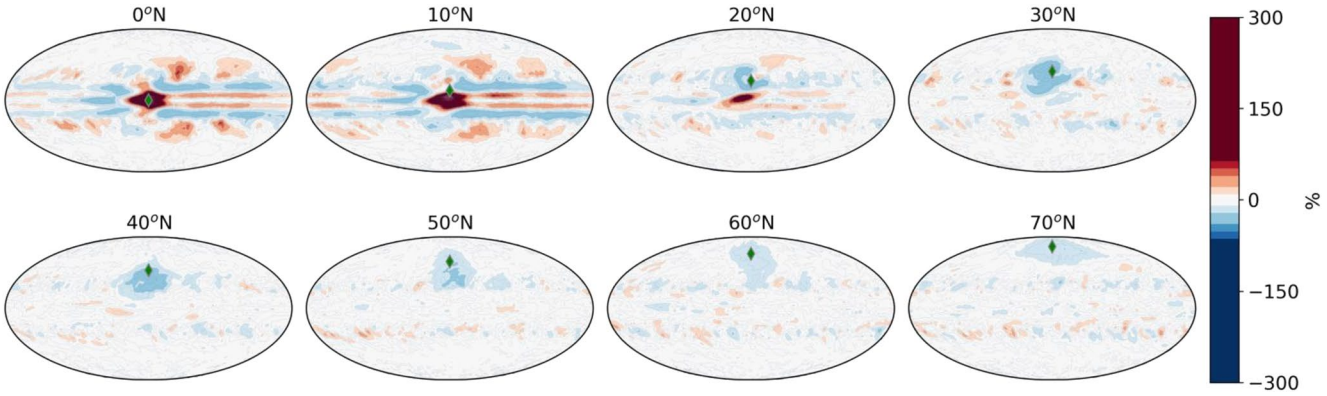

Figure 3. The relative precipitation change (compared to the reference simulation) for the aqua-planet simulations. For each simulation the aerosol plume center is indicated in the title and is marked by a green diamond.

To further understand why the transition between positive to negative response occurs at ~10°N, we present the Rossby radius of deformation (L_R) in the aqua-planet reference simulation in Figure 6. L_R is calculated as:

$$L_R = \frac{\left(\frac{gH\Delta\theta}{\theta_0}\right)^{0.5}}{f} \quad (2)$$

where g is the gravitational acelaration, H is the tropospheric height (the tropopause–defined as the first vertical level for which the temperature raises with height–Figure S6, hence the sharp transition at ~40°N), $\Delta\theta$ is the potential temperature difference between the tropopause and the surface (θ_0), and f is the Coriolis parameter. Figure 6 demonstrates that L_R decreases from infinity at the equator to about the Earth radius (a = 6,371 km) at 10°N. When $L_R > a$, a large scale direct thermally driven circulation can be generated as a response to diabatic heating (Dagan et al., 2019b; Roeckner et al., 2006; Stuecker et al., 2020). That is to say, that the mass field adjusts to the diabatic-heating, i.e., mass converges into the heating anomaly (see Figures S7–S8), which then generates vertical motion and supports an increase in precipitation. On the other hand, at latitudes higher than 10°, for which $L_R < a$, geostrophic adjustment of the flow confines the heating perturbations, generating a cyclonic circulation (of the size of L_R) around the plume center (Figure S9). We note that tropical cyclones, which required sufficient Coriolis force to form, are being generated outside of the deep tropics for the same reason (Gray, 1975).

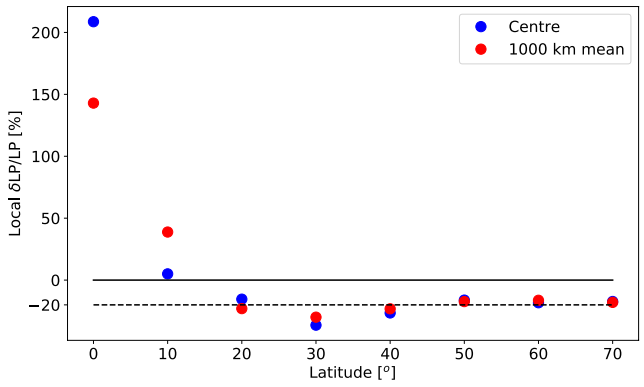

Figure 4. The relative precipitation change (compared to the reference simulation) at the center of the aerosol plume (blue) and the average relative precipitation change in a 1,000 km circle around the plume center (red) as a function of the center latitude location in the aqua-planet simulations. Black solid and dashed horizontal lines mark the 0% and 20% levels, respectively, for reference.

3.2. Fast Aerosol Effect on Precipitation over Land and Ocean

To investigate the similarities and differences between aerosol radiative effects on precipitation over land and ocean we use the AMIP simulations. In the AMIP configuration the SST is prescribed but the land surface temperature is allowed to react to the surface energy budget. This enables investigation of the fast effect (only over land) of aerosol-driven surface temperature changes (which drive changes in Q_{SH}) on precipitation. As a first step, we force the model with a similar idealized, large aerosol perturbation as in the aqua-planet simulations, in the tropics and extra-tropics, over the ocean or land (Figure 1). In this case we use either absorbing (SSA = 0.8) or scattering (SSA = 1) aerosols. Figure 7 presents the Q_R perturbations in these simulations and demonstrates a small perturbation in the case of scattering aerosol and a large and positive perturbation in the case of absorbing aerosols.

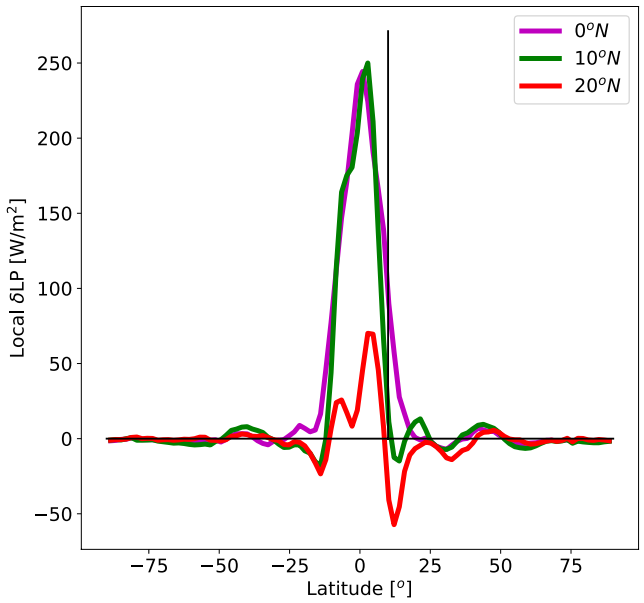

Figure 5. Meridional cross-sections of the precipitation response (compared to the reference simulation) at the longitude of the plume center for the aqua-planet simulations in which the plume center is at 0°N, 10°N and 20°N. The black vertical line marks a latitude of 10°N.

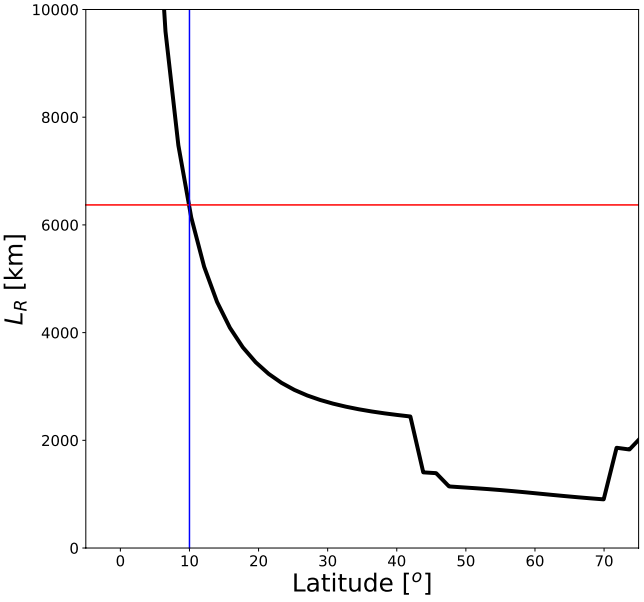

Figure 6. Rossby-radius of deformation as a function of latitude in the aqua-planet reference simulation. The blue vertical line marks a latitude of 10°N, while the red horizontal line markes the Earth radius (6,371 km).

Figures 8 and 9 present the precipitation and Q_{SH} response to the aerosol perturbations. It demonstrates a decrease in precipitation due to scattering aerosols over land in both the tropics and extra-tropics, concomitantly with a reduction in Q_{SH} (over the extra-tropics). This is in agreement with previous studies (e.g., Ramanathan et al., 2001). On the other hand, over the ocean, in a fixed SST configuration (fast precipitation response), scattering aerosols have no effect on either the precipitation or Q_{SH}. Like in the case of absorbing aerosols, we note that in the case of scattering aerosols over the tropics the local energy budget is not closed and requires large-scale convergence of energy (the opposite sign as in the case of absorbing aerosols, which generate large-scale divergence of energy). This efficient large-scale energy transport is supported in the tropics (Gill, 1980; Matsuno, 1966; Sobel et al., 2001) much more than in the extra-tropics, in which the local energy budget is closer to balance.

Absorbing aerosol perturbation over the ocean, unsurprisingly, generates a similar response as in the aqua-planet configuration (a positive precipitation response in the tropics and a negative response in the extra-tropics, without a large effect on Q_{SH}). Over land, as in the aqua-planet case, the precipitation response to absorbing aerosols is negative in the extra-tropics and a negative Q_{SH} response is also seen. This negative Q_{SH} response is caused by a reduction of the solar radiation reaching the surface and warming of the atmosphere due to the aerosol shortwave absorption. Over tropical land, the absorbing aerosol perturbation generates a more complex precipitation response. In the case of absorbing aerosols over South-America, the precipitation response is mostly negative over land and positive over the adjacent oceans. Over Africa the precipitation response is more positive over land (although there are places in which it is negative) and, as in the South-America case, positive and larger over the adjacent oceans. The smaller precipitation response to absorbing aerosol over tropical land (compared to over the ocean) can be understood by the fact that the negative Q_{SH} response (Figure 9) counteracts some of the positive Q_R tendency to generate direct thermally driven circulation. In addition, we note that the positive precipitation response over the east-tropical Atlantic is accompanied by a negative response over the west-tropical Atlantic. This is due to a zonal overturning circulation formed due to the aerosol effect leading to upward motion in the east Atlantic and downward motion in the west (see Figures S10–S11). A similar zonal response of a negative precipitation perturbation west of the plume center (in which there is a positive precipitation response) is seen in the aqua-planet simulations (see Figure 3, plume center at 0° and 10°), in the simulations with the absorbing aerosol plume over South-America (showing a decrease in precipitation over the central-tropical Pacific), and over the tropical Pacific (showing a decrease in precipitation over the Maritime Continent region). In the AMIP simulations there is an additional asymmetry introduced by land. As the precipitation has a strong seasonal cycle in many places (Figure S12), the response also shows a similar cycle (Figures S13–S16), however, the general trend does not change with the seasons.

Figures 10 and 11 present the surface temperature and pressure response to scattering and absorbing aerosol perturbation, respectively, over the extra-tropics (when SSTs are fixed the surface pressure is much less affected by aerosol perturbations over the tropics than over the extra-tropics due to the mass field adjustment). It demonstrates that both scattering and absorbing aerosols cause a reduction in surface temperature over land due to a reduction in surface shortwave radiation. However, a similar negative surface temperature perturbation drives a differing surface

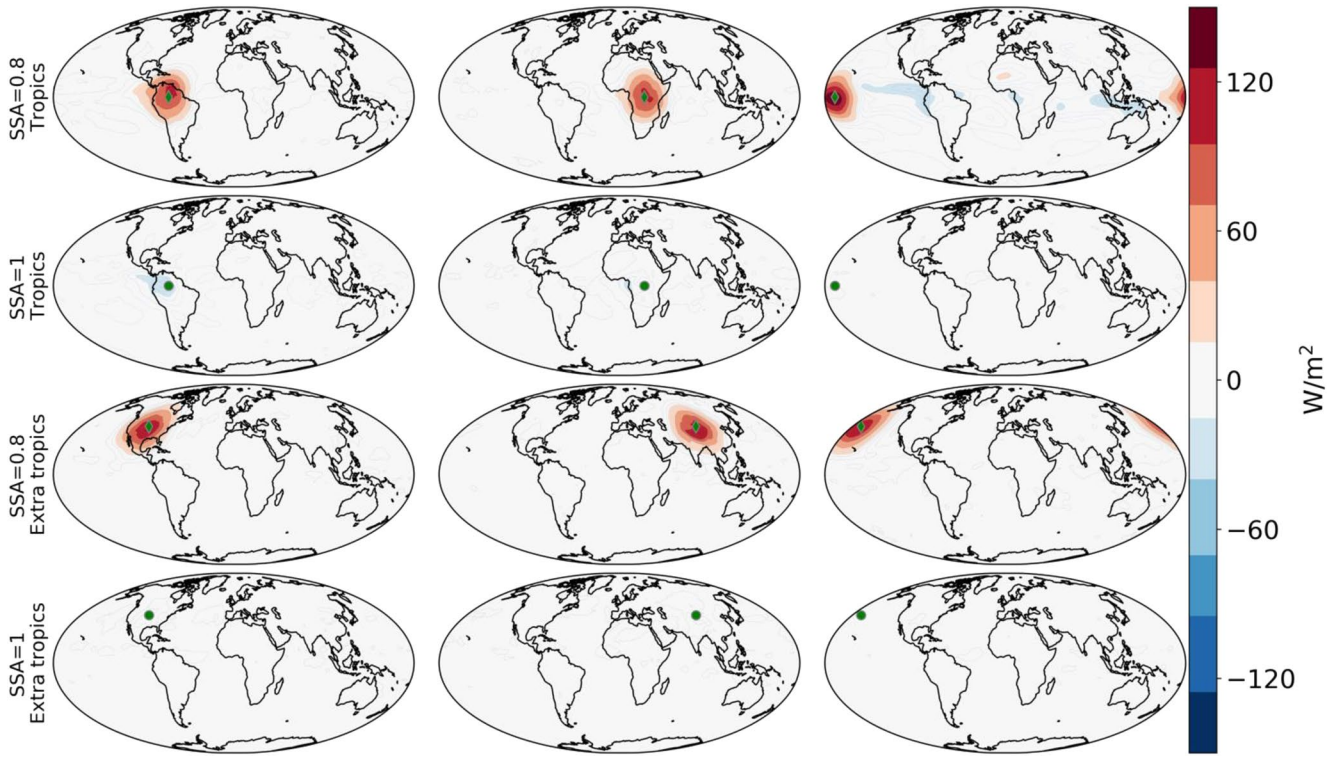

Figure 7. The atmospheric radiative heating (Q_R) perturbation (each simulation minus the reference simulation) in the AMIP simulations forced by idealized aerosol perturbation. For each simulation the aerosol plume center is marked by a green indicator–circles for scattering aerosol (SSA = 1) and diamonds for absorbing aerosols (SSA = 0.8). AMIP, Atmospheric Model Inter-comparison Project; SSA, single scattering albedo.

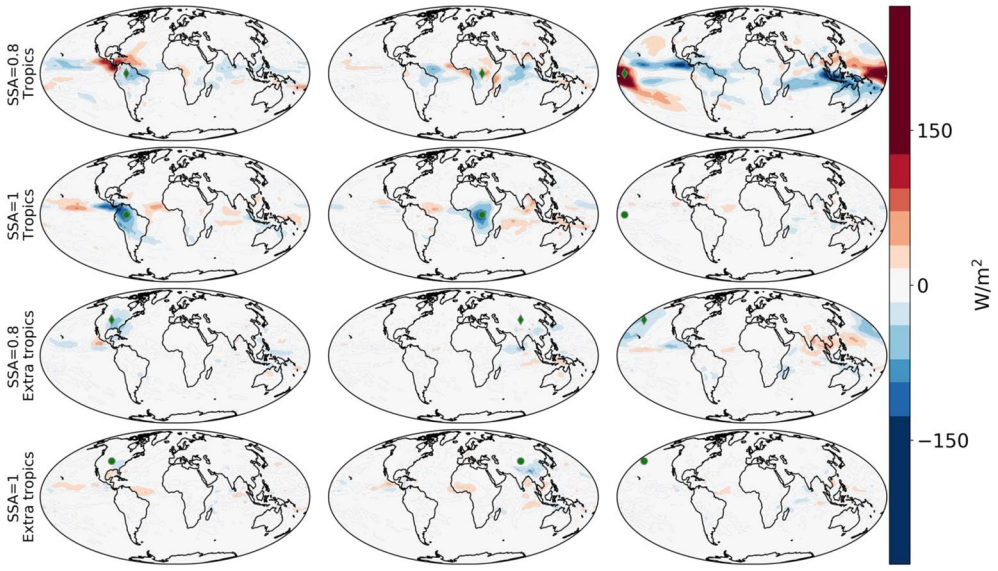

Figure 8. The precipitation latent heating change (compared to the reference simulation) in the AMIP simulations forced by idealized aerosol perturbation. For each simulation the aerosol plume center is marked by a green indicator–circles for scattering aerosol (SSA = 1) and diamonds for absorbing aerosols (SSA = 0.8). AMIP, Atmospheric Model Inter-comparison Project; SSA, single scattering albedo.

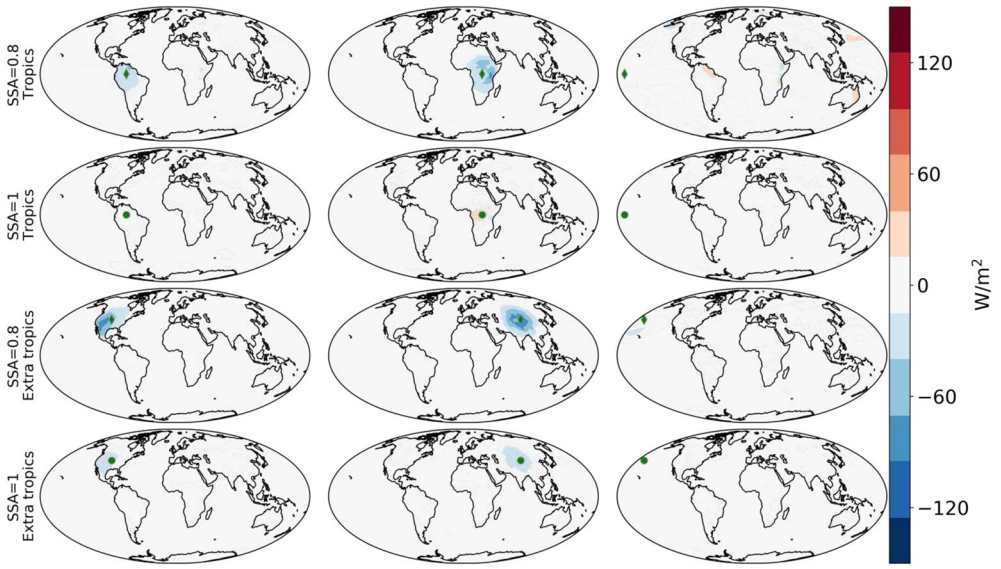

Figure 9. The sensible heat flux (Q_{SH}) change (compared to the reference simulation) in the AMIP simulations forced by idealized aerosol perturbation. For each simulation the aerosol plume center is marked by a green indicator–circles for scattering aerosol (SSA = 1) and diamonds for absorbing aerosols (SSA = 0.8). AMIP, Atmospheric Model Inter-comparison Project; SSA, single scattering albedo.

pressure response of an increase in the case of scattering aerosols (Figure 10) and a slight decrease in the case of absorbing aerosols (Figure 11). Over the ocean the surface temperature is not allowed to change so the surface pressure does not change much in the case of scattering aerosols (Figure 10), but decreases significantly in the case of absorbing aerosols (Figure 11).

To better understand these results, we examine zonal and meridional cross-sections of the temperature (T) and the pressure vertical wind (ω) responses in the simulations with the plume located over North-America, as an example (Figures 12 and 13, Figures S10–S11 present similar cross-sections for the simulations in

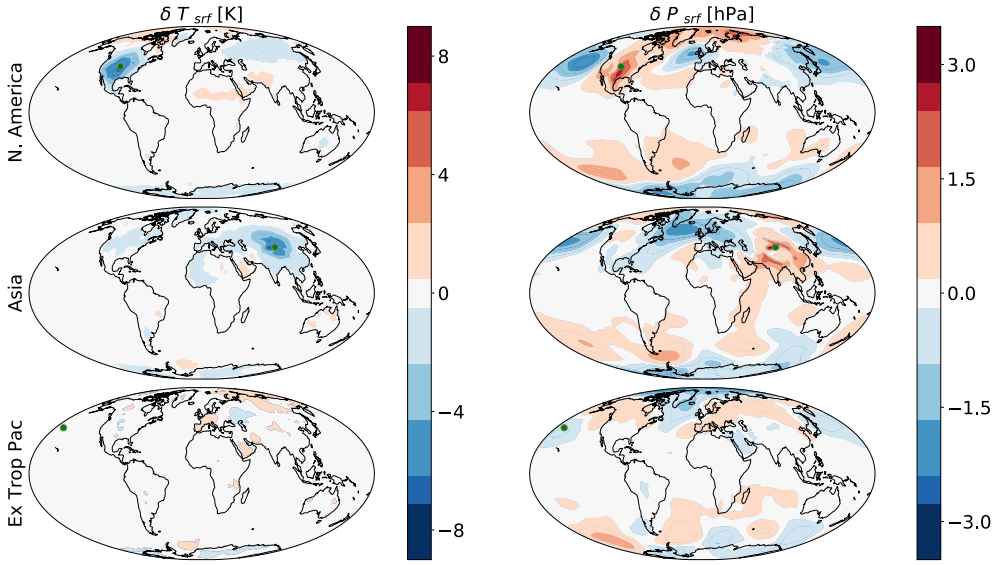

Figure 10. The surface temperature change (δT_{srf}–compared to the reference simulation, left column), and the surface pressure change (δP_{srf} - right column) in the AMIP simulations forced by idealized aerosol perturbation located at the extra-tropics with scattering aerosols (SSA = 1). For each simulation the aerosol plume center is marked by a green circle. AMIP, Atmospheric Model Inter-comparison Project; SSA, single scattering albedo.

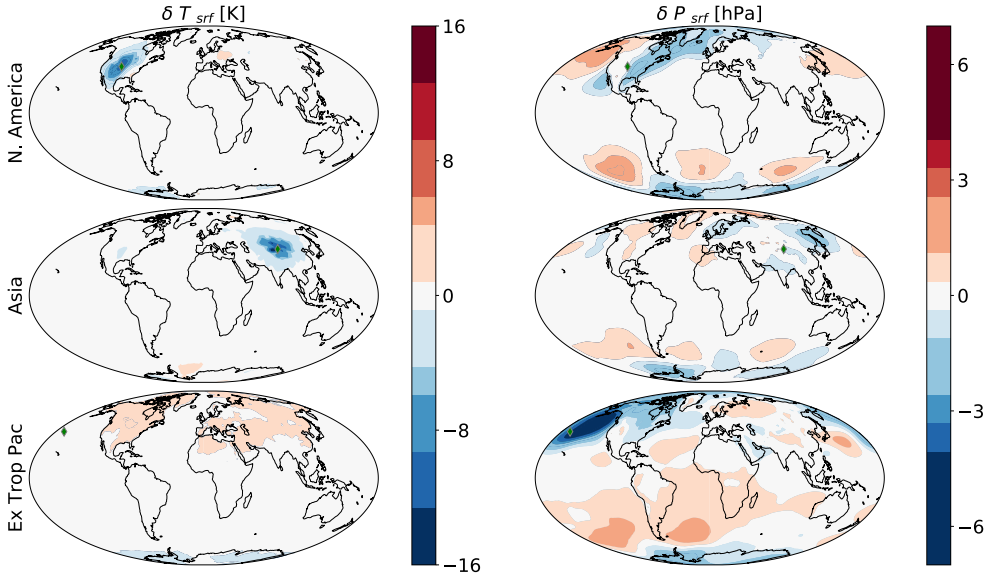

Figure 11. The surface temperature change (δT_{srf}–compared to the reference simulation, left column), and the surface pressure change (δP_{srf} - right column) in the AMIP simulations forced by idealized aerosol perturbation located at the extra-tropics with absorbing aerosols (SSA = 0.8). For each simulation the aerosol plume center is marked by a green diamond. AMIP, Atmospheric Model Inter-comparison Project; SSA, single scattering albedo.

which the aerosol plume is located over Africa as an example of a tropical aerosol plume, while the vertical profile of aerosol is presented in Figure S3). These results demonstrate that scattering aerosols lead to a cooling of both the surface and the entire troposphere. This cooling of the atmospheric column causes an increase in surface pressure (Figure 10), and a positive ω perturbation (representing subsidence - Figures 12 and 13) and hence also a reduction in cloudiness and precipitation (Figure 8), effectively the opposite of a classical "heat low". In the case of absorbing aerosols, on the other hand, the temperature is reduced near the surface (due to the reduction in surface shortwave radiation - see also Figure 11) and increased above (due to the direct effect of the absorbing aerosols). This contrasting temperature response with height leads to the small (mostly negative) surface pressure response (Figure 11) and to stabilization of the lower atmosphere, and hence reduction of precipitation. In addition, in both cases (absorbing and scattering aerosols), the subsidence is accompanied by surface divergence (Figure S17).

To sum up this section, in the case of absorbing aerosols, the effect of land reduces both the positive fast precipitation response in the tropics and the negative fast response in the extra-tropics due to the larger effect of Q_{SH} (compared to over the ocean), which counteracts the diabatic heating. In the case of scattering aerosols, the absence of any diabatic heating leads to a reduction in precipitation over tropical and extra-tropical lands due to the reduction in surface shortwave radiation.

3.3. Fast Aerosol Effect on Precipitation under More Realistic Perturbations

So far, we examined the precipitation response to idealized and very strong aerosol perturbations. This is useful for understanding the underlying physics (and a common practice in research of aerosol effect on precipitation, e.g., Myhre et al., 2017). However, one needs to remember that the effect of a more realistic perturbation, even if the same physics applies, may be obscured by natural variability (and also by other external forcings operating at the same time such as green-house gases). In order to examine whether a similar response, as in the idealized perturbations case, can be detected under a more realistic perturbation, we use the default MACv2-SP setup, which is based on observed anthropogenic aerosol perturbation. We note that using a non-interactive SST (as in the AMIP configuration) reduces some of the internal-variability of the climate system, hence, these simulations serves as a best case for detectability of the fast aerosol effect on precipitation. As a first step we use idealized, but broadly realistic aerosol plumes in each simulation, representing different geographical locations and different aerosol properties, to examine whether or not

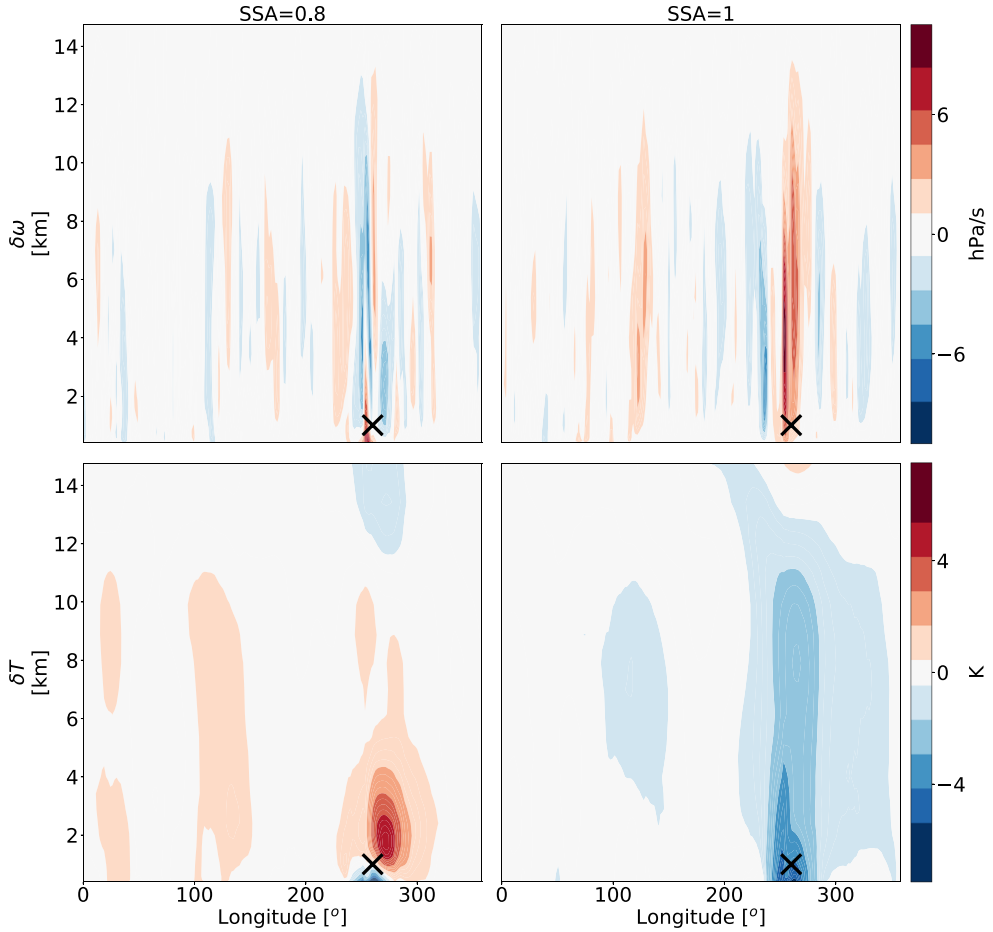

Figure 12. Zonal cross-sections of vertical wind ($\delta\omega$) and temperature (δT) differences from the reference simulation at the latitude of the center of the aerosol plumes (marked by "x") over North-America. The left column presents the simulation with absorbing aerosols (SSA = 0.8), while the right column presents the simulation with scattering aerosols (SSA = 1). SSA, single scattering albedo.

the response is consistent with the results described above. The aerosol plumes that we use are: The two African plumes (representing relatively absorbing aerosols mostly over tropical land), the Maritime Continent plume (representing relatively absorbing aerosols mostly over tropical ocean), the two Asian plumes (representing relatively scattering aerosols centered outside the deep-tropics but spending also into the deep-tropics–latitudes lower than 10°, mostly over land) and the European plume (representing relatively scattering aerosols mostly over extra-tropical land - Table 1). Figures S18–S19, present the horizontal and vertical AOD distribution in the different plumes.

Figure 14 presents the Q_R perturbation generated by forcing the model with each plume separately and the precipitation and Q_{SH} response to this perturbation. It demonstrates that, in the tropics, a positive Q_R perturbation due to absorbing aerosols generates a positive precipitation response. This is in agreement with the results from the idealized perturbations above. We note that the precipitation response over the ocean (in the case of the Maritime Continent plume and the adjacent ocean in the African case) is stronger than the response over land (Africa). As was explained above, the smaller precipitation response over land (compared to over the ocean) is due to the reduction in Q_{SH}, which weakens the formation of the thermally driven circulation. As in the idealized perturbation, the positive precipitation response over the eastern tropical Atlantic, generated by the African plumes, drives a negative response over the western tropical Atlantic due to a formation of zonal overturning circulation leading to upward motion in the east Atlantic and downward motion in the west (Figures S10–S11).

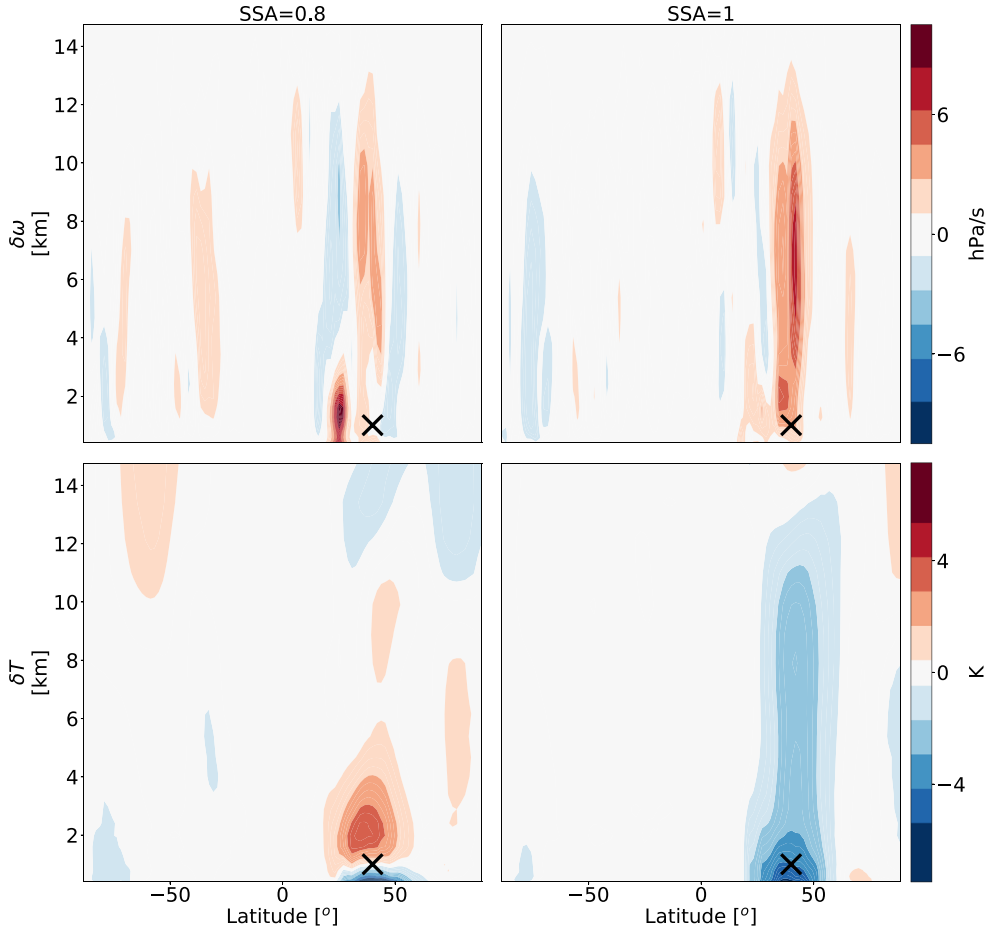

Figure 13. Meridional cross-sections of vertical wind ($\delta\omega$) and temperature (δT) differences from the reference simulation at the latitude of the center of the aerosol plumes (marked by "x") over North-America. The left column presents the simulation with absorbing aerosols (SSA = 0.8), while the right column presents the simulation with scattering aerosols (SSA = 1). SSA, single scattering albedo.

In the simulation which is forced by the two Asian plumes, the precipitation increases at the southern part of the plume, over the Indian ocean (reaching all the way to the deep-tropics), while it decreases over the northern part of the plumes over east Asia (over land). This, again, is in agreement with the general trend presented above based on the idealized perturbation, of an increase in precipitation in the deep-tropics and a decrease outside the deep-tropics. In addition, we note here again a larger tendency toward a positive response over tropical oceans than over tropical lands due to the role of Q_{SH}. The reduction in precipitation over land occurs mostly during the summer (Figure S20, the month with the maximum precipitation in the reference simulation, Figure S12) as the monsoon circulation weakens (Li et al., 2015). The European plume, which is confined to the extra-tropics, generates a weak Q_R perturbation due to a relatively low AOD and a high SSA. This weak Q_R is accompanied by a reduction in Q_{SH} and a negligible precipitation response. We believe that the precipitation response in this case is negligible because the perturbation is weak. To demonstrate it, we have run the model again with only the European plume but with 10 times larger AOD. Under this larger perturbation we do get a reduction in precipitation over Europe as predicted by the idealized perturbation simulation (Figure S21). However, the fact that we do not detect any significant reduction in precipitation over Europe in our simulations

Table 1
Names Followed Stevens et al. (2017), Location of Center and SSA (Single Scattering Albedo) of the Individual Plumes Used to Force the Model (the Two African and Two Asian Plumes are Used Together)

Source region	Latitude	Longitude	SSA at 550 nm
South central Africa	−3.5	16.0	0.87
North Africa	3.5	22.5	0.87
Maritime Continent	−1.0	106.0	0.87
South Asia	23.3	88.0	0.93
East Asia	30.0	114.0	0.93
Europe	49.4	20.6	0.93

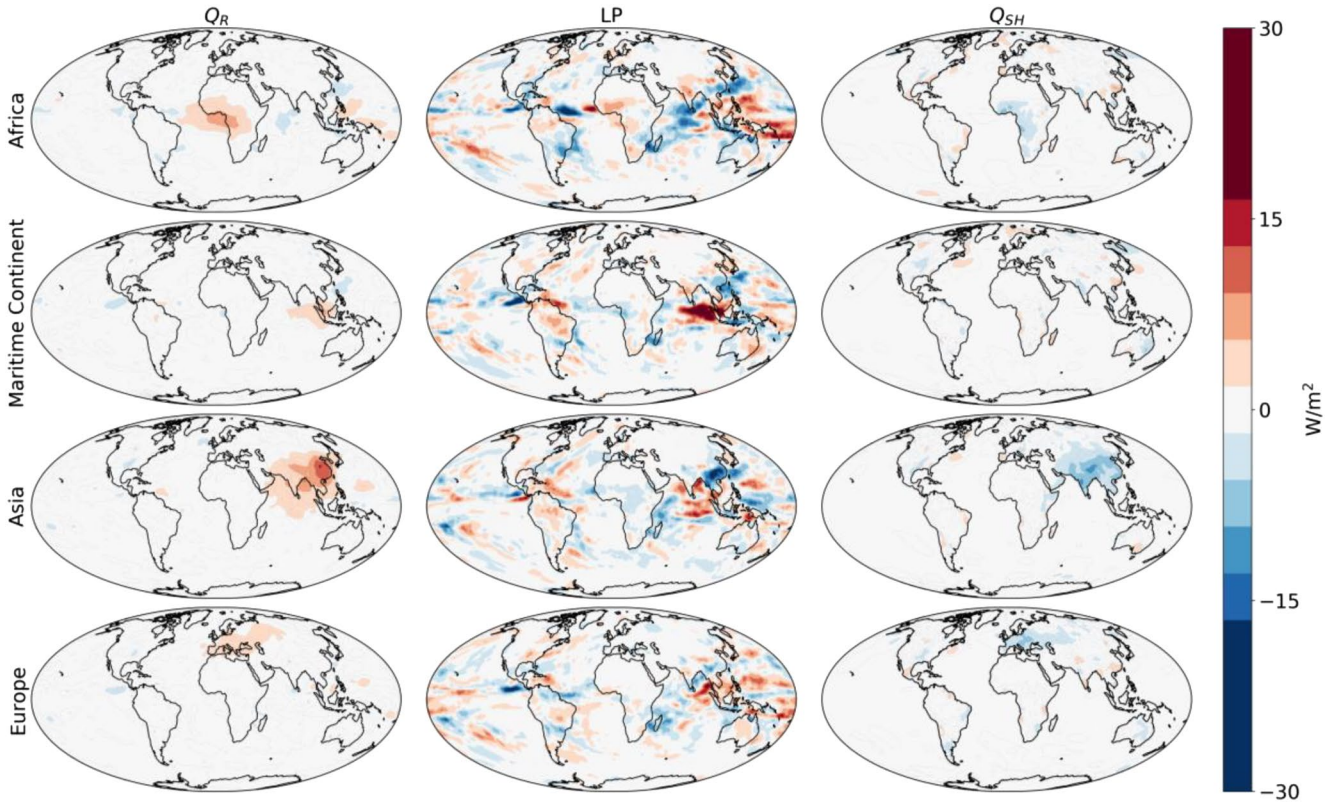

Figure 14. The atmospheric radiative heating (Q_R) perturbation (each simulation minus the reference simulation–left column), the precipitation latent heating change (middle column), and the sensible heat flux (Q_{SH}) change (right column) in AMIP simulations forced by individual aerosol plumes (based on Stevens et al., 2017). The individual plumes considered here are as listed in Table 1. AMIP, Atmospheric Model Inter-comparison Project.

suggest that the magnitude of a realistic perturbation is not sufficient to cause a reduction in precipitation that could be observed.

Examining regional precipitation response to local aerosol perturbation for different locations (Figure 14) reduces the role of teleconnections. Namely, aerosol perturbation at a given location could affect precipitation at other locations as well due to changes in the large-scale dynamics and thermodynamics of the atmosphere (Allen et al., 2015; Chemke & Dagan, 2018; Dagan & Chemke, 2016; Rotstayn & Lohmann, 2002; Voigt et al., 2017; Wang, 2015). To include these effects and to account for the global aerosol distribution we run the model with the full default MACv2-SP setup (Stevens et al., 2017), which includes, on top of the six aerosol plumes listed in Table 1, plumes over south and north America and over Australia (see Figure 1 in Stevens et al., 2017). Figure 15 presents the precipitation response in this simulation (Full plume). It demonstrates many similar features as in the individual plume experiments above, as well as in the idealized perturbation simulations. For example, it demonstrates an increase in precipitation over the tropical Indian ocean, a region forced by both the "Maritime Continent" plume and the south part of the "South Asia" plume. We also note a decrease in precipitation over East-Asian land and the adjacent ocean, as in the Asian plumes simulation. Figure 15 also shows an increase in precipitation over the eastern-tropical Atlantic Ocean (although less so over land), and a decrease in precipitation in the western-tropical Atlantic, a similar response as in the African plume simulation. However, the precipitation response is noisy and generally not statistically significant (p-value < 0.05 according to a *t*-test).

Since the Full plume experiment demonstrates precipitation changes which are generally in agreement with the idealized perturbation and the single plume experiments, we believe that the fact that it is not statistically significant is a matter of signal-to-noise ratio (the response is not significant compared to the natural variability, even for prescribed SST). This is demonstrated by simulations in which the AOD is increased (increasing the AOD at the center of each plume by a factor of 2, 5, and 10 to increase the signal-to-noise

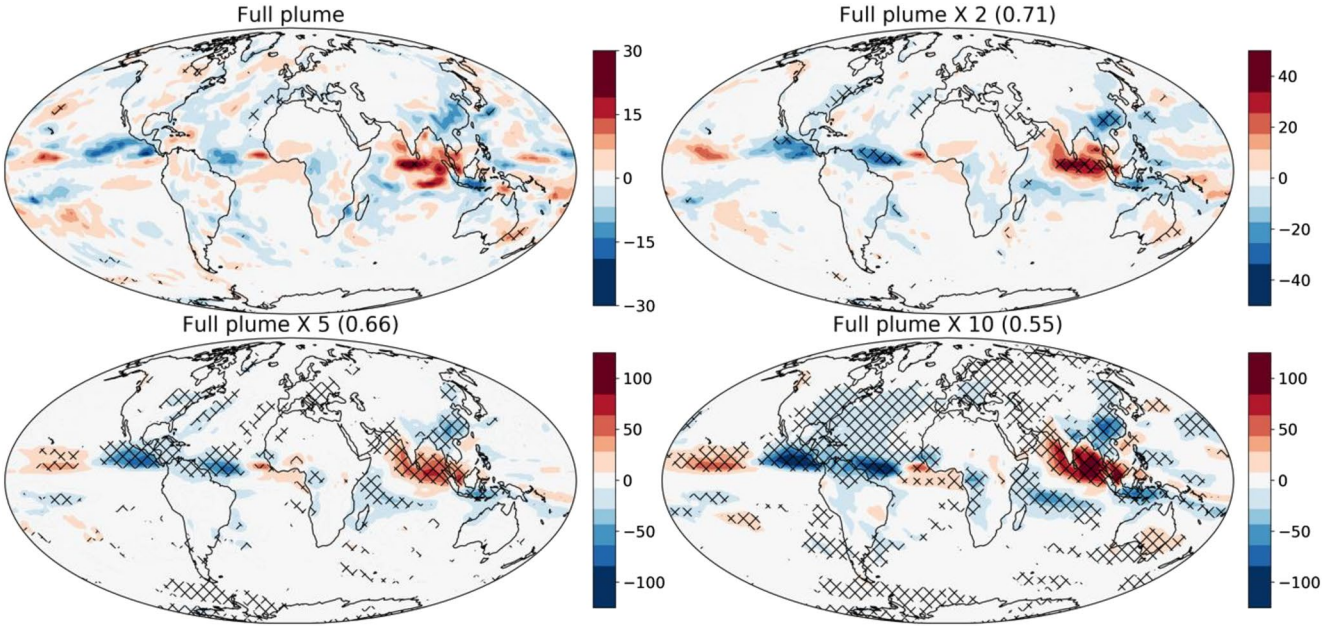

Figure 15. The precipitation latent heating change (compared to the reference simulation - W/m^2), in the AMIP simulations forced by the full global distribution of aerosols for a few levels of AOD compared to the Full plume simulation (indicated in the title of each subplot). The spatial correlation of each simulation with the Full plume simulation is indicated in the parenthesis. Locations in which the precipitation change is statistically significant (p-value < 0.05 according to a *t*-test) are marked with crosses. Please note the different color-bar for each subplot. Figure S22 presents the relative precipitation change in these simulations. AMIP, Atmospheric Model Inter-comparison Project; AOD, aerosol optical depth.

ratio–Figure 15). The spatial correlation of the precipitation response is relatively high between the higher AOD simulations and the Full plume simulation (0.71, 0.66 and 0.55 for the 2, 5, and 10 times AOD simulations) indicating a similar spatial structure. However, the precipitation response (with the similar spatial structure) becomes more statistically significant as the AOD increases. This suggests that the response seen in the Full plume simulation is mostly due to a robust physical driver, but is not strong enough to emerge from the model's natural variability (over a 30-year period with prescribed SST). Assuming that the model accurately represents the natural verbality of the atmosphere, these results may suggest that the aerosol-radiation effect on precipitation over the last few decades will be hard to detect from observations (although the slow response might be more important over this time-period and is not accounted for here). We note that running the model for a longer period than 30 years might increase the signal-to-noise ratio, however, 30 years is already quite long period for examining the fast precipitation response, as SST changes could become important on that time-scales (Scannell et al., 2019).

4. Summary

Precipitation changes due to anthropogenic activity are hard to predict despite their importance for society (Allan et al., 2020; Dagan et al., 2019a; Knutti & Sedláček, 2013; Myhre et al., 2017). One anthropogenic driver for precipitation changes are aerosols, which can affect the amount of precipitation through interacting with clouds or with radiation. In this study, we examine fast precipitation changes (not mediated by changes in SST) due to aerosol-radiation interaction using a global model with idealized aerosol perturbations of different levels of complexities. Specifically, we expand the analysis of a previous study (Dagan et al., 2019b), which demonstrated a contrasting precipitation response in the tropics and extra-tropics based on aqua-planet simulations. The goals of the current study are three-fold, however, all related to the geographical location of the aerosol perturbation: (1) to identify the latitude in which a transition between a local positive aerosol-driven precipitation response to a negative precipitation response occurs and explain why, (2) to examine the effect of land on the precipitation response, and (3) to examine the main conclusions under a more realistic aerosol perturbation in terms of magnitude and spatial structure. In this study we focus on the fast precipitation response (Bony et al., 2013; Myhre et al., 2018; Richardson et al., 2018) and

the related physical mechanisms. In a future study, we will examine the same trends in simulations with interactive SST, investigating the slow response.

Using idealized aqua-planet simulations with a stepwise increase in the absorbing aerosol plume latitude we show that the transition between a local increase and a decrease in precipitation occurs at relatively low latitudes of ~10°. Equatorward of ~10°, the Coriolis effect is negligibly low (the Rossby radius of deformation is larger than the earth radius), enabling a direct thermally driven circulation in response to aerosol diabatic heating (Dagan et al., 2019b; Roeckner et al., 2006). Poleward of ~10°, the Coriolis force is already sufficient to prevent the direct thermally driven circulation and a geostrophic adjustment of the flow confines the heating perturbations. Hence, the local precipitation is reduced to maintain energy balance. We note the similarity with tropical cyclogenesis (Gray, 1975), which requires sufficient Coriolis force to form cyclonic-circulation and to prevent the air from converging into the center. Hence, tropical cyclones do not form within a few degrees away of the equator.

Next, we examine the effect of land using AMIP type of simulations with idealized aerosol perturbation (large magnitude and idealized spatial structure). These results demonstrate that, in the case of absorbing aerosols, the effect of land is to reduce both the positive precipitation response in the tropics and the negative response in the extra-tropics due to the reduction of the surface sensible heat flux. This reduction in sensible heat flux over land counteracts the diabatic heating caused by absorbing aerosols and therefore reduces the effect as compared to over the ocean. In the case of scattering aerosols in the extra-tropics, surface cooling leads to a subsidence and an increase in surface pressure. The subsidence drives a reduction in cloudiness and precipitation. In the tropics, the surface pressure is less effected, but the reduction in surface shortwave radiation (due to scattering aerosols) drives a reduction in precipitation.

The fast precipitation response is also examined under more realistic aerosol perturbations (in terms of magnitude and spatial extent). This demonstrates that many of the physical insights gained by the idealized simulations can explain the fast precipitation response under more realistic conditions. For example, we show that the absorbing aerosol perturbation near the equator (over Africa and Maritime Continent region) generates an increase in precipitation mostly over the ocean and less so over land (due to the role of the sensible heat flux). We also show that in the case of an aerosol perturbation over Asia, which extends all the way from the deep-tropics to the extra-tropics, the precipitation response is positive near the equator over the ocean and negative over land outside the deep-tropics. In the case of the realistic magnitude perturbation over Europe, we show that no precipitation response is seen and we demonstrate that this is because of a small perturbation (relatively low AOD with relatively high SSA). Forcing the model with a stronger perturbation (increasing the AOD over Europe by 10 times) generate a local reduction in precipitation, as predicted by the idealized simulations.

We note that the vertical structure of the aerosol distribution may cause different responses of the climate system and general circulation (Ban-Weiss et al., 2012; Kim et al., 2015; Ming et al., 2010; Persad et al., 2012). Here we use a vertical distribution of aerosol which is based on a long-time average climatological data set (Kinne et al., 2013; Stevens et al., 2017). Over long time scales, in all cases, the AOD vertical profile shows a general reduction from the low altitudes (the source) to the mid-troposphere (the aerosols are mostly confined to below 5 km–Figure S19). Hence, in our simulations the variations of the vertical aerosol profiles are low and thus also the sensitivity to these variations.

In the last part of this paper, we force the model with the entire global distribution of aerosols, which includes changes in the large-scale circulation as well as teleconnections (Allen et al., 2015; Chemke & Dagan, 2018; Rotstayn & Lohmann, 2002; Shindell et al., 2010; Voigt et al., 2017; Wang, 2015) in addition to the local response due to changes in the energy budget. This demonstrates that many of the precipitation change features mentioned above are still relevant when the global aerosol distribution is included. However, the precipitation changes are shown to be statistically non-significant (for 30 years of simulations with a prescribed SST). We show that the fact that the precipitation changes are not statistically significant is not because it is inconsistent with our physical understanding of the system but because of a low signal-to-noise ratio. This is demonstrated through simulations in which the magnitude of the perturbation (AOD) is increased continually up to 10 times the default set-up, which is based on observations (Stevens

et al., 2017). The precipitation changes under stronger perturbations have a similar (although not identical) spatial structure and are shown to be more statistically significant.

Data Availability Statement

The data presented in this manuscript can be found online (10.5281/zenodo.4448345).

Acknowledgments
This research was supported by the European Research Council (ERC) project constRaining the EffeCts of Aerosols on Precipitation (RECAP) under the European Union's Horizon 2020 research and innovation program with grant agreement No 724602. The simulations were performed using the ARCHER UK National Supercomputing Service. D. Watson-Parris receives funding from the European Union's Horizon 2020 research and innovation program iMIRACLI under Marie Skłodowska-Curie grant agreement No 860100. DWP also gratefully acknowledges funding from the NERC ACRUISE project NE/S005390/1.

References

Albrecht, B. A. (1989). Aerosols, cloud microphysics, and fractional cloudiness. *Science*, *245*(4923), 1227–1230. https://doi.org/10.1126/science.245.4923.1227

Allan, R. P., Barlow, M., Byrne, M. P., Cherchi, A., Douville, H., Fowler, H. J., et al. (2020). Advances in understanding large-scale responses of the water cycle to climate change. *Annals of the New York Academy of Sciences*, *1472*, 49–75. https://doi.org/10.1111/nyas.14337

Allen, R. J., Evan, A. T., & Booth, B. B. B. (2015). Interhemispheric aerosol radiative forcing and tropical precipitation shifts during the late twentieth century. *Journal of Climate*, *28*(20), 8219–8246. https://doi.org/10.1175/jcli-d-15-0148.1

Allen, R. J., & Sherwood, S. C. (2011). The impact of natural versus anthropogenic aerosols on atmospheric circulation in the Community Atmosphere Model. *Climate Dynamics*, *36*(9–10), 1959–1978. https://doi.org/10.1007/s00382-010-0898-8

Andreae, M. O., Rosenfeld, D., Artaxo, P., Costa, A. A., Frank, G. P., Longo, K. M., & Silva-Dias, M. A. F. (2004). Smoking rain clouds over the Amazon. *Science*, *303*(5662), 1337–1342. https://doi.org/10.1126/science.1092779

Ban-Weiss, G. A., Cao, L., Bala, G., & Caldeira, K. (2012). Dependence of climate forcing and response on the altitude of black carbon aerosols. *Climate Dynamics*, *38*(5-6), 897–911. https://doi.org/10.1007/s00382-011-1052-y

Bony, S., Bellon, G., Klocke, D., Sherwood, S., Fermepin, S., & Denvil, S. (2013). Robust direct effect of carbon dioxide on tropical circulation and regional precipitation. *Nature Geoscience*, *6*(6), 447. https://doi.org/10.1038/ngeo1799

Chemke, R., & Dagan, G. (2018). The effects of the spatial distribution of direct anthropogenic aerosols radiative forcing on atmospheric circulation. *Journal of Climate*, *31*(17), 7129–7145. https://doi.org/10.1175/jcli-d-17-0694.1

Crueger, T., Giorgetta, M. A., Brokopf, R., Esch, M., Fiedler, S., Hohenegger, C., et al. (2018). ICON-A, The Atmosphere Component of the ICON Earth System Model: II. Model Evaluation. *Journal of Advances in Modeling Earth Systems*, *10*, 1638–1662. https://doi.org/10.1029/2017ms001233

Dagan, G., & Chemke, R. (2016). The effect of subtropical aerosol loading on equatorial precipitation. *Geophysical Research Letters*, *43*(20). https://doi.org/10.1002/2016gl071206

Dagan, G., Christensen, M., Stier, P., Seifert, A., Klocke, D., & Cioni, G. (2020). Atmospheric energy budget response to idealized aerosol perturbation in tropical cloud systems. *Atmospheric Chemistry and Physics*, *20*(7). https://doi.org/10.5194/acp-20-4523-2020

Dagan, G., Koren, I., & Altaratz, O. (2015). Aerosol effects on the timing of warm rain processes. *Geophysical Research Letters*, *42*(11), 4590–4598. http://dx.doi.org/10.1002/2015GL063839

Dagan, G., & Stier, P. (2020). Constraint on precipitation response to climate change by combination of atmospheric energy and water budgets. *npj Climate and Atmospheric Science*, *3*(1), 1–5. https://doi.org/10.1038/s41612-020-00137-8

Dagan, G., Stier, P., & Watson-Parris, D. (2019a). Analysis of the atmospheric water budget for elucidating the spatial scale of precipitation changes under climate change. *Geophysical Research Letters*, *46*, 10504–10511. https://doi.org/10.1029/2019GL084173

Dagan, G., Stier, P., & Watson-Parris, D. (2019b). Contrasting response of precipitation to aerosol perturbation in the tropics and extra-tropics explained by energy budget considerations. *Geophysical Research Letters*, *46*, 7828–7837. https://doi.org/10.1029/2019GL083479

Gates, W. L. (1992). AMIP: The Atmospheric Model Intercomparison Project. *Bulletin of the American Meteorological Society*, *73*(12), 1962–1970. https://doi.org/10.1175/1520-0477(1992)073<1962:atamip>2.0.co;2

Gill, A. E. (1980). Some simple solutions for heat-induced tropical circulation. *Quarterly Journal of the Royal Meteorological Society*, *106*(449), 447–462. https://doi.org/10.1002/qj.49710644905

Giorgetta, M. A., Brokopf, R., Crueger, T., Esch, M., Fiedler, S., Helmert, J., et al. (2018). ICON-A, the atmosphere component of the ICON Earth System Model. Part I: Model description. *Journal of Advances in Modeling Earth Systems*, *10*, 1613–1637. https://doi.org/10.1029/2017MS001242

Gray, W. M. (1975). *Tropical cyclone genesis* (p. 234). Atmospheric science paper.

Hodnebrog, O., Myhre, G., Forster, P. M., Sillmann, J., & Samset, B. H. (2016). Local biomass burning is a dominant cause of the observed precipitation reduction in southern Africa. *Nature Communications*, *7*. http://dx.doi.org/10.1038/ncomms11236

Jakob, C., Singh, M. S., & Jungandreas, L. (2019). Radiative convective equilibrium and organized convection: An observational perspective. *Journal of Geophysical Research - D: Atmospheres*, *124*(10), 5418–5430. https://doi.org/10.1029/2018jd030092

Khain, A. P. (2009). Notes on state-of-the-art investigations of aerosol effects on precipitation: A critical review. *Environmental Research Letters*, *4*(1), 015004. https://doi.org/10.1088/1748-9326/4/1/015004

Kim, H., Kang, S. M., Hwang, Y.-T., & Yang, Y.-M. (2015). Sensitivity of the climate response to the altitude of black carbon in the northern subtropics in an Aquaplanet GCM. *Journal of Climate*, *28*(16), 6351–6359. https://doi.org/10.1175/JCLI-D-15-0037.1

Kinne, S., O'Donnel, D., Stier, P., Kloster, S., Zhang, K., Schmidt, H., et al. (2013). MAC-v1: A new global aerosol climatology for climate studies. *Journal of Advances in Modeling Earth Systems*, *5*(4), 704–740. https://doi.org/10.1002/jame.20035

Knutti, R., & Sedláček, J. (2013). Robustness and uncertainties in the new CMIP5 climate model projections. *Nature Climate Change*, *3*(4), 369. https://doi.org/10.1038/nclimate1716

Levin, Z., & Cotton, W. R. (2009). Aerosol pollution impact on precipitation. In Z. Levin, & W. R. Cotton (Eds.), A scientific review. Springer.

Li, X., Ting, M., Li, C., & Henderson, N. (2015). Mechanisms of Asian summer monsoon changes in response to anthropogenic forcing in CMIP5 models*. *Journal of Climate*, *28*(10), 4107–4125. https://doi.org/10.1175/jcli-d-14-00559.1

Liu, H., Guo, J., Koren, I., Altaratz, O., Dagan, G., Wang, Y., et al. (2019). Non-monotonic aerosol effect on precipitation in convective clouds over tropical oceans. *Scientific Reports*, *9*(1), 7809. https://doi.org/10.1038/s41598-019-44284-2

Liu, L., Shawki, D., Voulgarakis, A., Kasoar, M., Samset, B. H., Myhre, G., et al. (2018). A PDRMIP Multimodel Study on the impacts of regional aerosol forcings on global and regional precipitation. *Journal of Climate*, *31*(11), 4429–4447. https://doi.org/10.1175/jcli-d-17-0439.1

Matsuno, T. (1966). Quasi-geostrophic motions in the equatorial area. *Journal of the Meteorological Society of Japan*, *44*(1), 25–43. https://doi.org/10.2151/jmsj1965.44.1_25

Ming, Y., Ramaswamy, V., & Chen, G. (2011). A model investigation of aerosol-induced changes in boreal winter extratropical circulation. *Journal of Climate*, *24*(23), 6077–6091. https://doi.org/10.1175/2011jcli4111.1

Ming, Y., Ramaswamy, V., & Persad, G. (2010). Two opposing effects of absorbing aerosols on global-mean precipitation. *Geophysical Research Letters*, *37*(13). https://doi.org/10.1029/2010gl042895

Muller, C. J., & O'Gorman, P. A. (2011). An energetic perspective on the regional response of precipitation to climate change. *Nature Climate Change*, *1*(5), 266. https://doi.org/10.1038/nclimate1169

Myhre, G., Forster, P. M., Samset, B. H., Hodnebrog, Ø., Sillmann, J., Aalbergsjø, S. G., et al. (2017). PDRMIP: A Precipitation Driver and Response Model Intercomparison Project-Protocol and Preliminary Results. *Bulletin of the American Meteorological Society*, *98*(6), 1185–1198. https://doi.org/10.1175/bams-d-16-0019.1

Myhre, G., Kramer, R., Smith, C., Hodnebrog, Ø., Forster, P., Soden, B., et al. (2018). Quantifying the importance of rapid adjustments for global precipitation changes. *Geophysical Research Letters*, *45*(20), 11399–311405. https://doi.org/10.1029/2018gl079474

Persad, G. G., Ming, Y., & Ramaswamy, V. (2012). Tropical tropospheric-only responses to absorbing aerosols. *Journal of Climate*, *25*(7), 2471–2480. https://doi.org/10.1175/jcli-d-11-00122.1

Ramanathan, V., Crutzen, P., Kiehl, J., & Rosenfeld, D. (2001). Aerosols, climate, and the hydrological cycle. *Science*, *294*(5549), 2119–2124. https://doi.org/10.1126/science.1064034

Rast, S. (2018). *Special configurations of the atmosphere*. Report on ICON. https://doi.org/10.5676/DWD_pub/nwv/icon

Richardson, T. B., Forster, P. M., Andrews, T., Boucher, O., Faluvegi, G., Fläschner, D., et al. (2018). Drivers of precipitation change: An energetic understanding. *Journal of Climate*, *31*(23), 9641–9657. https://doi.org/10.1175/jcli-d-17-0240.1

Roeckner, E., Stier, P., Feichter, J., Kloster, S., Esch, M., & Fischer-Bruns, I. (2006). Impact of carbonaceous aerosol emissions on regional climate change. *Climate Dynamics*, *27*(6), 553–571. https://doi.org/10.1007/s00382-006-0147-3

Rosenfeld, D., & Lensky, I. M. (1998). Satellite-based insights into precipitation formation processes in continental and maritime convective clouds. *Bulletin of the American Meteorological Society*, *79*(11), 2457–2476. https://doi.org/10.1175/1520-0477(1998)079<2457:sbiipf>2.0.co;2

Rotstayn, L. D., & Lohmann, U. (2002). Tropical rainfall trends and the indirect aerosol effect. *Journal of Climate*, *15*(15), 2103–2116. https://doi.org/10.1175/1520-0442(2002)015<2103:trtati>2.0.co;2

Samset, B. H., Myhre, G., Forster, P. M., Hodnebrog, Ø., Andrews, T., Faluvegi, G., et al. (2016). Fast and slow precipitation responses to individual climate forcers: A PDRMIP multimodel study. *Geophysical Research Letters*, *43*(6), 2782–2791. https://doi.org/10.1002/2016gl068064

Scannell, C., Booth, B. B. B., Dunstone, N. J., Rowell, D. P., Bernie, D. J., Kasoar, M., et al. (2019). The influence of remote aerosol forcing from industrialized economies on the future evolution of East and West African rainfall. *Journal of Climate*, *32*(23), 8335–8354. https://doi.org/10.1175/jcli-d-18-0716.1

Shindell, D., Schulz, M., Ming, Y., Takemura, T., Faluvegi, G., & Ramaswamy, V. (2010). Spatial scales of climate response to inhomogeneous radiative forcing. *Journal of Geophysical Research: Atmosphere*, *115*(D19). https://doi.org/10.1029/2010jd014108

Sobel, A. H., Nilsson, J., & Polvani, L. M. (2001). The weak temperature gradient approximation and balanced tropical moisture waves*. *Journal of the Atmospheric Sciences*, *58*(23), 3650–3665. https://doi.org/10.1175/1520-0469(2001)058<3650:twtgaa>2.0.co;2

Stevens, B., Fiedler, S., Kinne, S., Peters, K., Rast, S., Müsse, J., et al. (2017). MACv2-SP: A parameterization of anthropogenic aerosol optical properties and an associated Twomey effect for use in CMIP6. *Geoscientific Model Development*, *10*, 433–452. https://doi.org/10.5194/gmd-10-433-2017

Stuecker, M. F., Timmermann, A., Jin, F.-F., Proistosescu, C., Kang, S. M., Kim, D., et al. (2020). Strong remote control of future equatorial warming by off-equatorial forcing. *Nature Climate Change*, *10*, 124–129. https://doi.org/10.1038/s41558-019-0667-6

Voigt, A., Pincus, R., Stevens, B., Bony, S., Boucher, O., Bellouin, N., et al. (2017). Fast and slow shifts of the zonal-mean intertropical convergence zone in response to an idealized anthropogenic aerosol. *Journal of Advances in Modeling Earth Systems*, *9*(2), 870–892. https://doi.org/10.1002/2016ms000902

Wang, C. (2015). Anthropogenic aerosols and the distribution of past large-scale precipitation change. *Geophysical Research Letters*, *42*, 10876–10884. https://doi.org/10.1002/2015GL066416

Zängl, G., Reinert, D., Rípodas, P., & Baldauf, M. (2015). The ICON (ICOsahedral Non-hydrostatic) modeling framework of DWD and MPI-M: Description of the non-hydrostatic dynamical core. *Quarterly Journal of the Royal Meteorological Society*, *141*(687), 563–579. https://doi.org/10.1002/qj.2378

Zhao, A. D., Stevenson, D. S., & Bollasina, M. A. (2019). The role of anthropogenic aerosols in future precipitation extremes over the Asian Monsoon Region. *Climate Dynamics*, *52*(9–10), 6257–6278. https://doi.org/10.1007/s00382-018-4514-7